Brief Papers

Discrete-Time Adaptive Windowing for Velocity Estimation

Farrokh Janabi-Sharifi, Vincent Hayward, and Chung-Shin J. Chen

***Abstract*—We present methods for velocity estimation from discrete and quantized position samples using adaptive windowing. Previous methods necessitate tradeoffs between noise reduction, control delay, estimate accuracy, reliability, computational load, transient preservation, and difficulties with tuning. In contrast, a first-order adaptive windowing method is shown to be optimal in the sense that it minimizes the velocity error variance while maximizes the accuracy of the estimates, requiring no tradeoff. Variants of this method are also discussed. The effectiveness of the proposed technique is verified in simulation and by experiments on the control of a haptic device.**

***Index Terms*—Adaptive windowing, best-fit, control enhancement, discrete-time position, filtering, haptic interface, velocity estimation.**

I. Introduction

NUMEROUS control systems require on-line velocity estimation from a discrete-time position signal. Examples include velocity control of manipulators [9], visual servoing [6], implementation of stiff virtual walls for force reflecting interfaces [4], as well as most guidance and tracking systems. Previous methods for real-time velocity estimation include: finite difference and inverse-time methods, filtered derivative, alpha-beta trackers, and Kalman filtering. All these methods share fundamental tradeoffs between: noise reduction and control delay; accuracy of the estimate and its reliability; as well as regarding the computational load. They also all might need tuning.

We describe here a class of adaptive finite impulse response (FIR) velocity estimation techniques which are optimal in the sense of minimizing the error variance while maximizing the accuracy of estimates, requiring no tradeoff. These techniques possess noise filtering properties but preserve the velocity transients. This is exemplified by applying the technique to the control enhancement of a haptic device in order to significantly increase the size of the region of allowable control gains.

Manuscript received July 8, 1997; revised April 3, 2000. Recommended by Associate Editor, W. Gruver. This work was supported by IRIS (Phase 2) under Project "Haptic Devices for Teleoperation and Virtual Environments" (HMI-6), the Institute for Robotics and Intelligent Systems part of Canada's National Centers of Excellence program (NCE), and an operating Grant "High Performance Robotic Devices" from the Natural Science and Engineering Research Council (NSERC) of Canada. The work of F. Janabi-Sharifi was supported by a post-doctoral fellowship from NSERC.

F. Janabi-Sharifi is with the Department of Mechanical Engineering, Ryerson Polytechnic University, Toronto, ON, M5B 2K3 Canada (e-mail: fsharifi@acs.ryerson.ca).

V. Hayward is with Center for Intelligent Machines, Department of Electrical and Computer Engineering, McGill University, Montréal, PQ, H3A 2A7 Canada (e-mail: hayward@cim.mcgill.ca).

C.-S. J. Chen was with McGill Center for Intelligent Machines, Department of Electrical and Computer Engineering, McGill University, Montréal, PQ, H3A 2A7 Canada. He is now with Extreme Packet Devices Inc., Kanata, ON, K2K 3A7, Canada.

Publisher Item Identifier S 1063-6536(00)07357-7.

II. Velocity Estimation

A position signal $x(t)$ is sampled with period T. x_k is the true position at time kT, and $y_k = x_k + e_k$ is the measurement with error e_k. The error may be due to quantization (encoders, digital converters) and other sources. In many cases, it is valid to assume that the error is bounded. In the absence of additional information, the error can be conservatively considered to have a zero mean bounded uniform distribution (e.g., the case of pure quantization), such that $-d \leq e_k \leq d$. This implies that

$$r = \mathrm{var}(e_k) = E[e_k^2] = \frac{d^2}{3}. \tag{1}$$

The problem we consider is to find an estimate $\hat{v}_k$ for $v = dx/dt$ from measurements $\{y_i\}_{k-n}^{k}$, with n to be the size of window. Used online, an estimation algorithm should reduce the effects of noise and minimize delay to avoid compromising the phase margin in closed-loop control. These objectives are in conflict with fixed filters. Moreover, the estimation should be computationally effective. A measure of performance used in this paper is the size of regions of allowable gains for PD control. Given a fixed computational resource, the higher the achievable sampling rate (the simpler the estimator), the larger the gains may be chosen.

A. Finite Difference and Inverse Time Methods

The finite difference method (FDM) uses Euler approximation

$$\hat{v}_k = \frac{y_k - y_{k-1}}{T} = \frac{x_k - x_{k-1}}{T} + \frac{e_k - e_{k-1}}{T}. \tag{2}$$

This method asymptotically breaks down at high sampling rates when high time-resolution is needed for feedback control. As T becomes smaller, the position increments decrease but the noisy component does not and is correspondingly amplified.

With the inverse-time approach [7], estimates of the velocity are obtained by dividing the interpulse angle from an encoder by the time between successive pulses. In this case, the opposite problem occurs, the basic quantum estimate of $1/v_k$ depends inversely on the position resolution and the scheme breaks down for high position resolution.

B. Kalman Filter

Another approach is to describe the system by discrete stochastic dynamical equations and to apply Kalman filtering (KF) [1]

$$\boldsymbol{x}_{k+1} = A\boldsymbol{x}_k + G\boldsymbol{w}_k \tag{3}$$

$$y_k = H\boldsymbol{x}_k + e_k. \tag{4}$$

Here $\boldsymbol{x}_k = (x_k, \dot{x}_k, \ddot{x}_k)^T$. The acceleration is dropped if a double integrator model is used. A and H are the state transition and observation matrices, respectively. In [1], it is shown that standard deviation of the velocity estimation with the triple integrator is two to four times better than in the case of the double integrator. We will use the triple integrator model for our simulations

$$A = \begin{bmatrix} 1 & T & \dfrac{T^2}{2} \\ 0 & 1 & T \\ 0 & 0 & 1 \end{bmatrix}, \quad H = [1 \quad 0 \quad 0]. \tag{5}$$

G is defined as the identity matrix and $\boldsymbol{w}_k = [w_1, w_2, w_3]^T$ represents the process noise. $\boldsymbol{w}_k$ and the measurement noise e_k are assumed to be zero mean white Gaussian. The covariance matrix of $\boldsymbol{w}_k$, Q_k is defined as

$$Q_k\delta_{kj} = E[\boldsymbol{w}_k\boldsymbol{w}_k^T] \tag{6}$$

where δ_{kj} is the Kronecker delta. $\boldsymbol{w}_k$ is viewed as a surrogate for either acceleration (double integrator) or its derivative (triple integrator) and therefore can be written as $Q_k = \mathrm{diag}[0, 0, q]$. Since actual motions are not well characterized by a stationary random process, q must be taken as a parameter to be adjusted. The variance for the measurement error e_k is given by (1). Since the covariance matrix of measurement noise is a scalar, we represent it by r. The discrete-time Kalman filter is then described by

$$\begin{aligned} \text{Prediction:} \quad & \hat{\boldsymbol{x}}_{k,k-1} = A\hat{\boldsymbol{x}}_{k-1,k-1} \\ & P_{k,k-1} = A P_{k-1,k-1} A^T + Q_k \\ \text{Gain:} \quad & K_k = P_{k,k-1} H_k^T [r + H_k P_{k,k-1} H_k^T]^{-1} \\ \text{Update:} \quad & \hat{\boldsymbol{x}}_{k,k} = \hat{\boldsymbol{x}}_{k,k-1} + K[y_k - H_k \hat{\boldsymbol{x}}_{k,k-1}] \\ & P_{k,k} = P_{k,k-1} - K H_k P_{k,k-1}. \end{aligned} \tag{7}$$

The Kalman filter provides optimal (minimum variance, unbiased) estimation of state $\boldsymbol{x}_k$ with the given observations $y_{k-1}, y_{k-2}, \ldots, y_0$ when the model for system dynamics and the measurement relation are perfect. When they are imperfect, the filter can learn the wrong state and the state estimation might diverge. Adaptive fading Kalman filter (AKF) can be used to eliminate the effect of older data using a forgetting factor $\lambda_k \geq 1$ in the error covariance equation [14]

$$P_{k,k-1} = \lambda_k A P_{k-1,k-1} A^T + Q_k. \tag{8}$$

Since the performance critically depends on λ_k, we use an optimal algorithm for computing it [14]. For our model, (A, G) is controllable and (A, H) is observable. Therefore $P_{k,k-1}$ is positive definite. P_0 and r, are positive definite, and Q can be made positive definite by adding a small positive scalar ϵ to its diagonal elements, H_k is row-wise full-ranked, so the optimal forgetting factor can be computed by

$$\lambda_k = \max\{1, \ \mathrm{trace}[N_k M_k^{-1}]\} \tag{9}$$

where

$$\begin{aligned} M_k &= H_k A P_{k-1,k-1} A^T H_k^T \\ N_k &= H_k P_{k,k-1} H_k^T - H_k Q_k H_k^T. \end{aligned} \tag{10}$$

The Kalman filter using the triple integrator model of (5) requires at least n^3 operations which might not be suitable for real-time applications. Also, tuning of the process noise covariance matrix is cumbersome and different operational conditions require retuning. Finally, the convergence of Kalman filter is not always guaranteed. Since the alpha–beta trackers comprise a specialized form of double integrator Kalman filter [10], they will not be further discussed in this paper.

C. Fixed Filter Methods

The idea is to assume that the noisy position signal can be separated into spectral components: a low-pass frequency component from which a velocity estimate can be reliably derived and a noisy component which must be filtered out. Fixed low-pass filters, such as Butterworth filters, evaluate the weighted sum of the filtered and raw velocity estimates from finite difference method [16], denoted by $\hat{v}_j$ and $\hat{v}'_j$, respectively

$$\hat{v}_k = \sum_{j=0}^{n} b_j \hat{v}'_{k-j} + \sum_{j=1}^{n} a_j \hat{v}_{k-j} \tag{11}$$

where a_j and b_j are the filter coefficients. As the order of the filter n increases, the filter approaches an ideal low-pass filter.

The design of fixed causal filters always faces fundamental tradeoffs between time lag, phase distortion, attenuation, and cutoff precision. Typically, they involve tuning for each application and operating condition, especially in closed loop since the filter becomes part of the system transfer function. Furthermore, the signal is filtered the same way the noise is: rapid changes in the input signal are attenuated, resulting in a poor transient response.

Fig. 1. Effect of window length on the variance of velocity.

III. Adaptive Windowing Techniques

Adaptive windowing is now discussed in the case of first-order fits.

A. First-Order Adaptive Windowing

It was seen that the Euler approximation applied to two position samples is more *precise* if they are far apart. This observation is graphically conveyed by Fig. 1. The larger the window length, the smaller the variance of the velocity is. This is equivalent to averaging the last n velocity estimates,

$\hat{v}_k$, $\hat{v}_{k-1}$, …, $\hat{v}_{k-n}$, with $\hat{v}_i$ obtained from the finite difference method (2)

$$\hat{v}_k = \frac{1}{n}\sum_{j=0}^{n-1} \hat{v}_{k-j} = \frac{y_k - y_{k-n}}{nT}. \tag{12}$$

Provided that the signal is well represented by its samples, increasing the window size is equivalent to decreasing the sampling rate. A large window introduces time delay and also reduces the estimation *reliability*.

In order to trade *precision* against *reliability*, the window size should be selected *adaptively* depending on the signal itself. The window size should be short when the velocity is high, yielding more reliable estimates and faster calculation; it should be large when the velocity is low so producing more precise estimates.

Noise reduction and precision put a lower bound on the window size, while reliability provides an upper limit for the window length. In other words, a criterion should be established to determine whether the slope of a straight line approximates reliably the derivative of a signal between two samples x_k, x_{k-n}. It can then be used to find the longest window which satisfies the accuracy requirement, solving a min–max problem.

As described shortly below, simple test can ensure that a straight line passing through y_k, y_{k-n} covers all intermediate samples given an uncertainty band defined by the peak norm of the noise $d = \|e_k\|_\infty$, $\forall k$. All the estimates in the set $[((y_k - y_{k-n})/nT) - (2\,d/nT), ((y_k - y_{k-n})/nT) + (2\,d/nT)]$ are probable, so a method must be found to pick one optimally, since its existence is ensured constructively. The smaller that set (the larger n), then the more precise is any one of them, provided that this estimate explains the data reliably.

The first proposal is "end-fit first-order adaptive windowing" (end-fit-FOAW). The solution can be stated as finding a window of length n where $n = \max\{1, 2, 3, \ldots\}$ such that

$$|y_{k-i} - {}^{L}y_{k-i}| \le d, \quad \forall\, i \in \{1, 2, \ldots, n\} \tag{13}$$

where ${}^{L}y_{k-i} = a_n + b_n(k-i)T$, given that

$$a_n = \frac{k y_{k-n} + (n-k) y_k}{n}, \quad \text{and} \quad \hat{v}_k = b_n = \frac{y_k - y_{k-n}}{nT}. \tag{14}$$

The optimality of the approach is justified by the following proposition.

Proposition 1: If a position trajectory has a piecewise continuous and bounded derivative, and if the measurement noise is uniformly distributed, the proposed method minimizes the velocity error variance and maximizes the accuracy of the estimate.

Proof: Consider a position trajectory χ that has piece-wise continuous and bounded derivative V. Denote the time derivative at instant k as v_k. If the measurement noise is uniformly distributed, from (12), it follows that

$$\hat{v}_k \in \left[\frac{y_k - y_{k-n}}{nT} - \frac{2\,d}{nT}, \frac{y_k - y_{k-n}}{nT} + \frac{2\,d}{nT}\right], \text{ or}$$

$$\hat{v}_k - \frac{2\,d}{nT} \le v_k \le \hat{v}_k + \frac{2\,d}{nT} \tag{15}$$

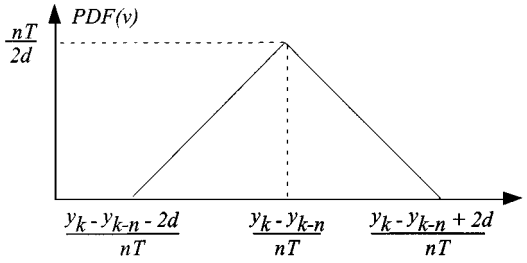

Fig. 2. PDF of velocity for window of length n.

which implies a probability density function (PDF) of the triangular form (Fig. 2) for the velocity with

$$\sigma^2_{v_k} = \frac{2\,d^2}{3n^2T^2}. \tag{16}$$

Therefore, the largest possible n will minimize the variance for the velocity error. Moreover, the slope of the line passing through the points y_k and y_{k-n} is the estimate of the maximum likelihood, $nT/2\,d$. □

The end-fit-FOAW estimator works as follows:

Step 1) Set $i = 1$.

Step 2) Set y_k as the last sample and y_{k-i} as the ith before y_k.

Step 3) Calculate b_n, slope of the line passing through y_k and y_{k-i} from (14).

Step 4) Check whether the line passes through all points inside the window within the uncertainty band of each point.

Step 5) If so, set $i = i + 1$ and GOTO Step 3). Else return the last estimate.

The end-fit-FOAW estimates the velocity using two position measurements. This causes undesired overshoots if the window size is small. To provide additional smoothing a best-fit estimate using all the samples in the window can be used instead. Then, the velocity estimate is the slope of a least-square approximation which minimizes the error energy, and hence is a natural choice.

The Best-fit-FOAW solution is the same as end-fit-FOAW solution except that in Step 3) above, b_n is calculated from

$$b_n = \frac{n\sum_{i=0}^{n} y_{k-i} - 2\sum_{i=0}^{n} i\, y_{k-i}}{T\,n(n+1)(n+2)/6}. \tag{17}$$

Similarly, it can be shown that the best-fit-FOAW is suboptimal. The quality of velocity estimation by best-fit-FOAW can be further improved. In a yet another heuristic variant, best-fit-FOAW-R, the window length determination is based on best-fitting lines on increasingly longer windows. So Step 3) uses (17).

B. Auxiliary Smoothing

It should be noted that the reliability criterion can be relaxed to account for the effects of outliers. An outlier is a rare event in the signal. A simple method to make the filter more robust to outliers is to stop the window growth if at least two consecutive sample fall out of the fit.

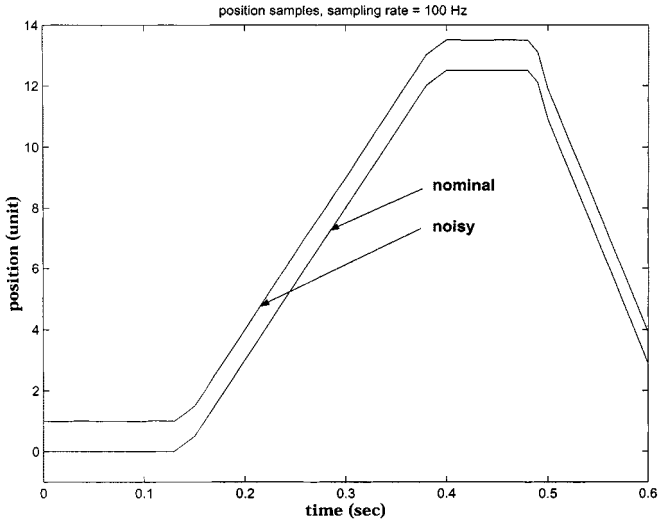

Fig. 3. The original and the noisy trajectories shifted by one unit.

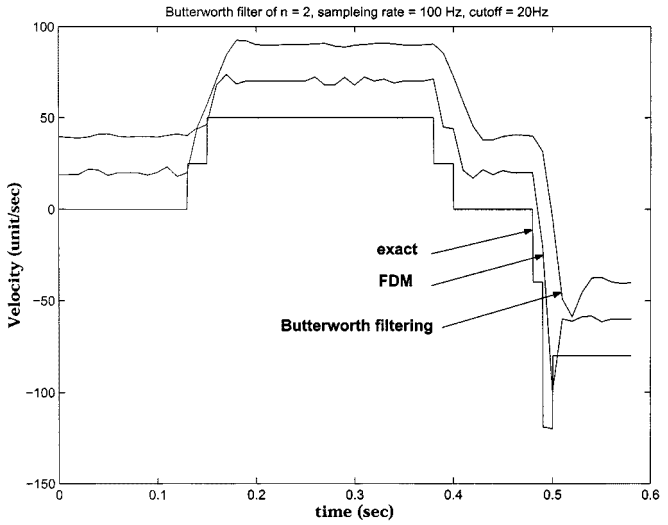

Fig. 4. The responses of FDM without and with a second-order Butterworth filter: sampling rate = 100 Hz, cutoff frequency = 20 Hz (FDM and Butterworth filtering trajectories have been shifted 20 and 40 units/s, respectively).

Fixed filters do not distinguish between the signal and unwanted noise: they attenuate the signal in the same way as they attenuate the noise component, masking the transients. One alternative is *median filtering* to preserve signal discontinuities while eliminating fine irregularities and outliers [15] because no averaging occurs. The window size needs not be large (a typical value is 5) for effectiveness.

IV. Simulation

The performance of the proposed methods is now compared with the other techniques. Evenly distributed noise (±5%) was added to a position signal sampled at 100 Hz for a test position trajectory comprising velocity steps, that is, acceleration impulses, see Fig. 3. Matlab was used for the simulations.

A. Fixed Filter versus FOAW

The effect of a second-order filter with cutoff frequency of 20 Hz can be seen on Fig. 4 by comparison to plain FDM and

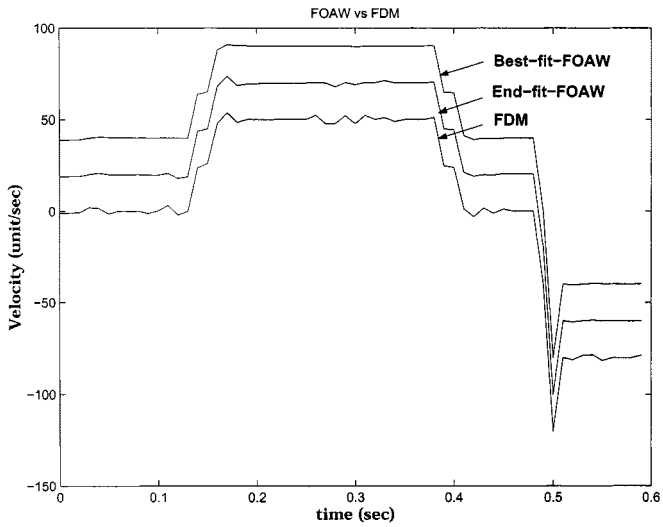

Fig. 5. The responses of FDM, end-fit-FOAW, and best-fit-FOAW (end-fit-FOAW and best-fit-FOAW results have been shifted 20 and 40 units/s, respectively).

to the exact velocity profile, where noise is attenuated with the cost of estimation lag. Higher cutoff frequencies are limited by the Nyquist rate.

Next, the End-fit-FOAW performance is compared with that of FDM (Fig. 5). The velocity noise is rejected considerably, there is almost no time lag, and the transients are preserved. The best-fit-FOAW further improves the quality of the velocity estimation, being less prone to overshoots.

B. Kalman Filter versus FOAW

The performance of FOAW was compared to that of KF on the same data. The triple integrator model of (4), (5) was used and the system states were predicted and updated by (7). The variance r was calculated from (1) to be 20.1×10^{-5} unit.. The first three measurements were used to initialize the $\hat{\boldsymbol{x}}_{0,0}$ vector. Using (1) and (2), it can be observed that the error covariances of $\hat{x}_{0,0}$ and $\hat{v}_{0,0}$ are $d^2/3$ and $2\,d^2/3T^2$, respectively. Similarly, the acceleration estimate can be found to be $2\,d^2/T^4$. Consequently, our initial error covariance is

$$P_0 = \operatorname{diag}\left[\frac{d^2}{3}, \frac{2\,d^2}{3T^2}, \frac{2\,d^2}{T^4}\right]. \tag{18}$$

The Kalman filter estimates for different q values were computed. It was found that $q = 2\times10^4$ provides the best compromise between overshoot and delay. From Fig. 6, best-fit-FOAW gives superior estimations although the filter was tuned for this trajectory. The performance of adaptive fading Kalman filtering (AKF) for velocity estimation was also compared with that of FOAW. The same value of $q = 2\times10^4$ was used. Fig. 6 indicates that the adaptive fading filter leads to smoother results. However, FOAW-based velocity estimates are still superior.

C. Effect of Auxiliary Smoothing

The final test was to compare the performance of the best-fit-FOAW with that of best-fit-FOAW-R, and to study the effect of median smoothing. Another position signal was generated by sampling at 600 Hz and adding an evenly distributed

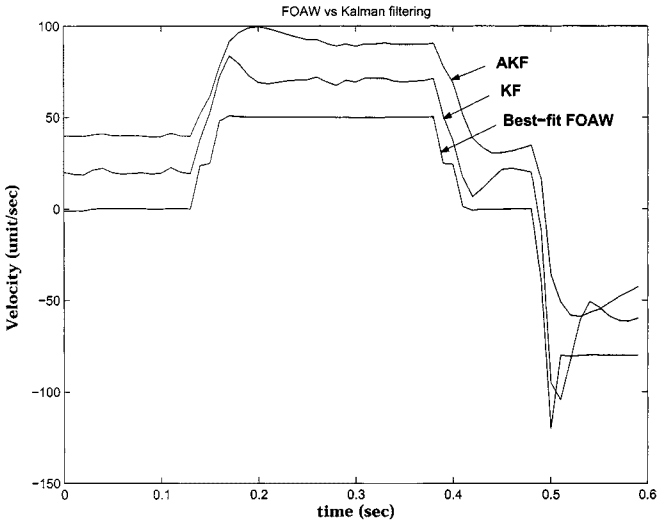

Fig. 6. The response of the three filters (the responses of KF and AKF have been shifted 20 and 40 units/s, respectively).

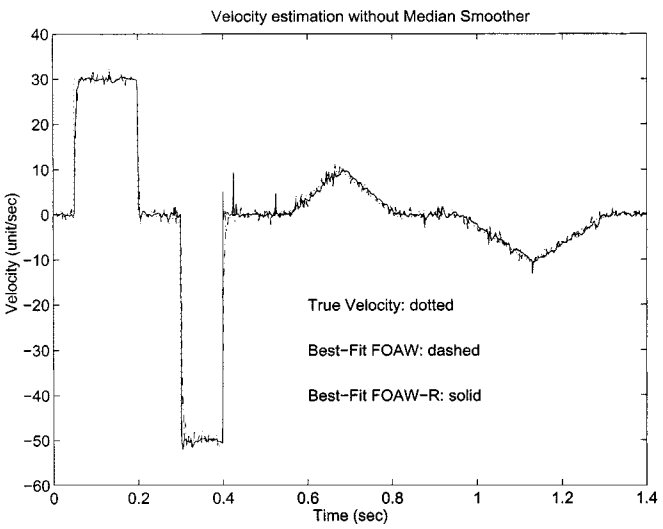

Fig. 7. Time transient performance of best-fit-FOAW methods.

noise ($d = 0.03$). An upper bound for the window size is set to be 15 to prevent excessive delays. Fig. 7 shows that both FOAWs preserve the transients but best-fit-FOAW-R estimates the velocity more accurately.

The position signal was then preprocessed by a median smoother. This further improved the velocity estimates as in Fig. 8. Median velocity smoothing after the estimation, as shown in Fig. 9, provides a slight advantage. It was noted that median smoothing of the velocity given by best-fit FOAW produces similar quality when compared to best-fit FOAW-R without median-smoothing. Best-fit-FOAW with median-smoothing (on velocity and/or position) may be used instead of best-fit FOAW-R to obtain comparable estimation quality.

V. Experimental Case Study

The proposed techniques have numerous applications, e.g., to haptic devices. These are mechanical devices that provide force feedback to enrich the interaction between a human operator

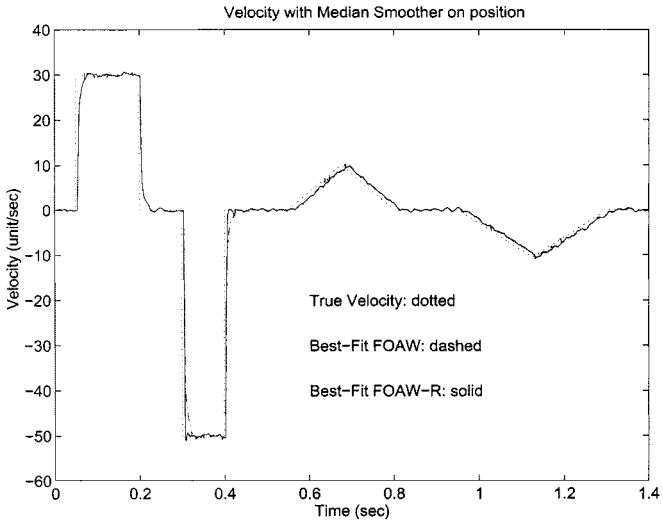

Fig. 8. Effect of median position-smoothing.

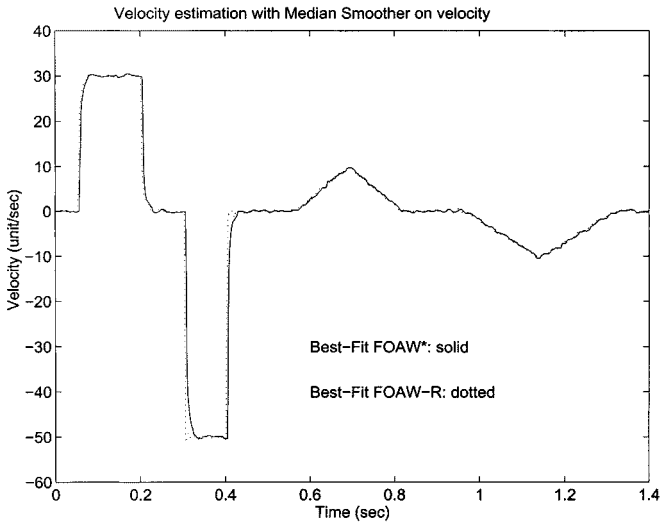

Fig. 9. Effect of velocity-smoothing.

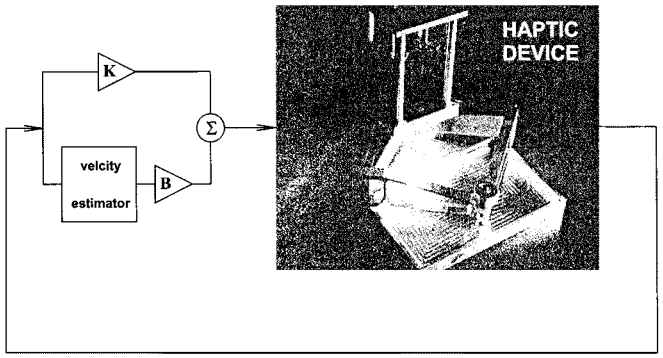

Fig. 10. Experimental setup.

and a machine. Some examples are human-computer interfaces [13], telerobotics, and gaming industries [12]. A virtual wall modeled by a spring with a stiffness constant (K) and a damper with a damping coefficient (B) is often taken as a benchmark test [3]. Such a case can be generally depicted in a block diagram as shown in Fig. 10. The virtual damping B in the model

provides passivity to the wall to combat the effect of sampling [5]. The differentiation operation, a high-pass filter, amplifies the damping noise and limits the possible values of K and B. Minsky *et al.* [11] found empirically the stability condition for virtual wall implementation to be of the form

$$\frac{B}{KT} > c. \tag{19}$$

In [2], using the Padé approximation, c was found to be 2/3 if the digital loop has one delay and a zero-order-hold. This shows that if K is large, B must be large too. A noisy estimate of the velocity will limit B and therefore K as well.

A two-degree-of-freedom haptic device, the Pantograph [8], was used for the experiment on achievable gains for K and B (Fig. 10). The position signal was fed back to the input of a discrete-time PD controller. The output is a torque command applied to a device which can be closely approximated by an inertia (very little friction and structural dynamics). The signal was left noisy (not more than eight stable bits out of 12). For certain values of K and B, the system entered stable limit cycles, for other values, the system becomes unstable. Stability and noise tests are conducted and are described below. The lower bound of the useful region is given by the amount of damping B that is required for each K to avoid a limit-cycle oscillatory behavior. The upper limit indicates the values of B which cause the noise to exceed a prescribed threshold for each K too. The onset of limit cycles was determined by applying an impulsive disturbance to the position of the device. The interior composite region outlines the useful region: a region where gain selections are at the same time free of limit cycles and free of noise. The results are presented in the style of [3].

In the first three plots (Fig. 11), three velocity estimation techniques (FDM, end-fit-FOAW, and best-fit-FOAW) are compared against each other, showing the effects of the sampling frequency on the system performance. In the next three plots (Fig. 12), the same performance regions for each algorithm are shown but varying the frequency (300, 800, 1500 Hz).

The following observations can be made.

1) Both FOAWs perform much better than FDM, especially when the sampling frequency is high. This is seen from the first three plots in Fig. 11. FOAW estimators raise the upper limit of B for all K's with an exception for some K's at the lowest frequency, 300 Hz. This can be explained by the fact that FDM approximates the true velocity well enough at low sampling rates.
2) For any sampling rate, these regions are enlarged with the use of FOAW estimators (with the largest area for the best-Fit-FOAW). This, in essence, shows the effectiveness of the FOAW algorithms. In general, a higher sampling rate results in larger errors and therefore, the effect of noise is more severe which consequently decreases the area of the usable region.
3) FOAW estimators yield an effective rejection of noise, and therefore result in a higher upper value of B, as compared to FDM. It also makes the system less susceptible to noise, especially at high frequencies, as shown in the flattening of upper bound B at 1500 Hz in the three plots of Fig. 12.

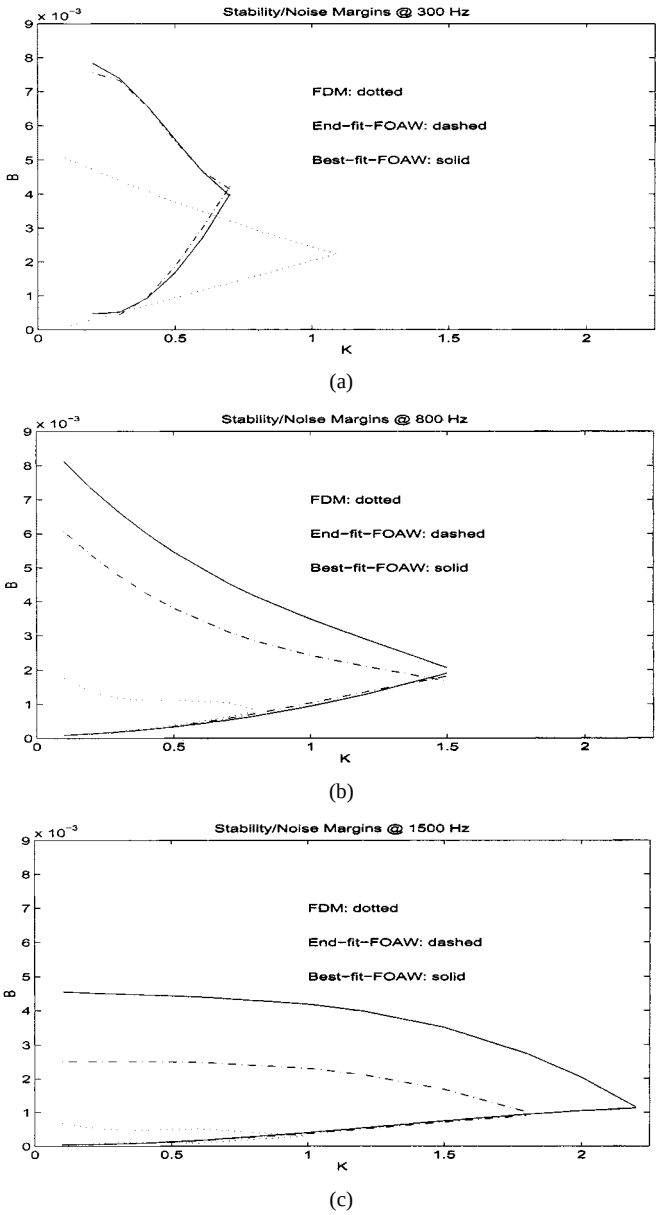

Fig. 11. Stability-noise regions for K and B with different estimation algorithms at (a) 300 Hz, (b) 800 Hz, and (c) 1500 Hz.

4) FOAW's do not introduce instabilities due to delay since the lower limits of the composite regions remain unchanged at a fixed sampling frequency as in plots of Fig. 11.
5) The lower bound of the useful region is lowered with increasing sampling rates which demonstrates the necessity of better estimators to combat the effects of noise as seen in plots of Fig. 12.

VI. Conclusion

The proposed methods demonstrated improved accuracy, time-transient, and control enhancement over existing techniques. The effectiveness of the proposed methods has been verified by simulation results and also by real-time experimental results in the control of a haptic device. It was concluded that, among the proposed methods, if the computational cost

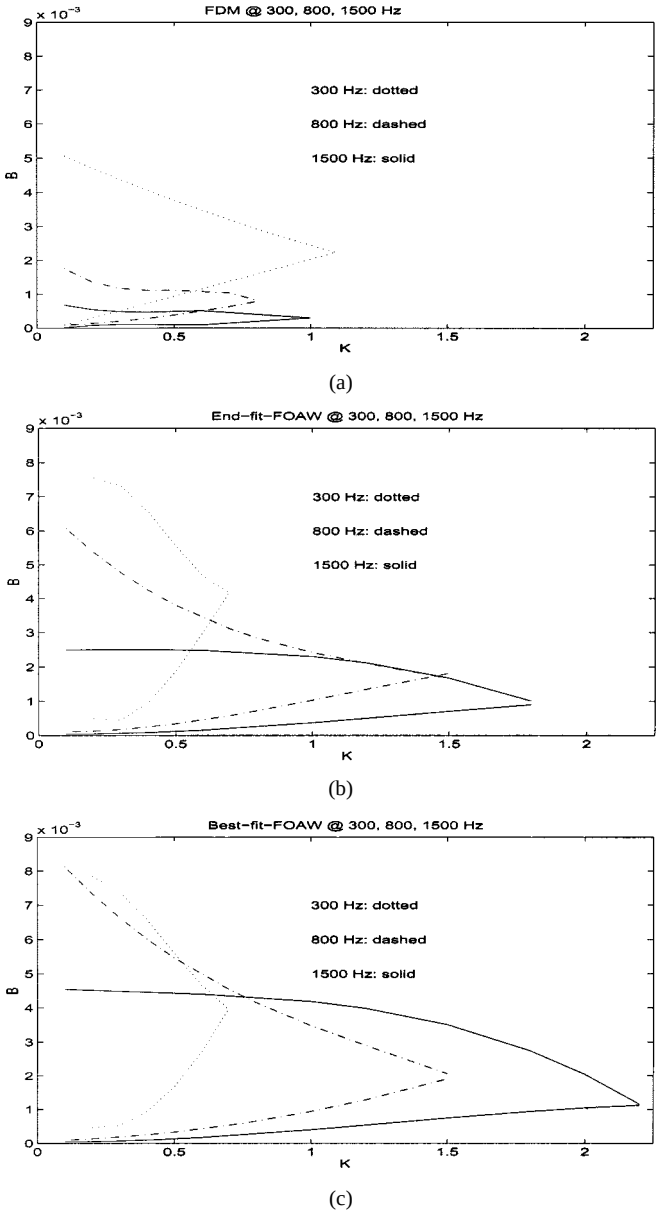

Fig. 12. Stability-noise regions for K and B at 300, 800, and 1500 Hz, for (a) FDM, (b) end-fit-FOAW, and (c) best-fit-FOAW.

is not a concern, best-fit-FOAW-R will provide more accurate velocity estimation. Otherwise, best-fit-FOAW with median smoothing may be used instead of best-fit-FOAW-R to give a quality velocity estimation.

It was also mentioned in the introduction that finite-different methods break down at low velocities (respectively, high rates) while inverse-time methods break down at high velocities (respectively, low rates). FOAW adapts to the signal so at low velocities it resembles the inverse-time method (since it measures the intervals between events which are far apart in time but close in space), while at high velocities it resembles the finite-difference method (since it measures events which are far apart in space but close in time). FOAW can also be considered from the view point of its transfer functions. When the velocity is high it is a filter of minimum order and when it is low it is a filter of maximum order which is lower pass.

ACKNOWLEDGMENT

The authors would like to thank R. Ellis from Queen's University and D. K. Pai from the University of British Columbia for stimulating initial discussions. The authors would also like to thank H. Najaf-Zadeh and N. Sheikholeslami from the digital signal processing group at McGill University for their helpful comments.

REFERENCES

[1] P. R. Bélanger, "Estimation of angular velocity and acceleration from shaft encoder measurements," in *Proc. IEEE Int. Conf. Robot. Automat.*, Nice, France, 1992, pp. 585–592.

[2] B. Bonneton and V. Hayward, "Implementation of a virtual wall," Center for Intelligent Machines, McGill Univ., Montreal, PQ, Canada, Tech. Rep., 1994.

[3] J. E. Colgate and J. M. Brown, "Factors affecting the Z-width of a haptic display," in *IEEE Int. Conf. Robot. Automat.*, 1994, pp. 3205–3210.

[4] J. E. Colgate, P. E. Grafing, M. C. Stanley, and G. Schenkel, "Implementation of stiff virtual walls in force-reflecting interfaces," in *Proc. IEEE Virtual Reality Annu. Int. Symp.*, 1993, pp. 202–208.

[5] J. E. Colgate and G. Schenkel, "Passivity of a class of sampled-data systems: Application to haptic interfaces," in *Proc. Amer. Contr. Conf.*, June 1994, pp. 37–47.

[6] P. I. Corke, "Dynamics of visual control," in *IEEE Int. Conf. Robot. Automat. Workshop Visual Servoing*, San Diego, CA, 1994.

[7] B. H. Habibullah, H. Singh, K. L. Soo, and L. C. Ong, "A new digital speed transducer," *IEEE Trans. Ind. Electron. Contr. Instrum.*, vol. IE-25, pp. 339–342, 1978.

[8] V. Hayward, J. Choksi, G. Lanvin, and C. Ramstein, "Design and multi-objective optimization of a linkage for a haptic interface," in *Advances in Robot Kinematics*, J. Lenarcic and B. Ravani, Eds. Boston, MA: Kluwer, 1994, pp. 352–359.

[9] A. Jaritz and M. W. Spong, "An experimental comparison of robust control algorithms on a direct drive manipulator," *IEEE Trans. Contr. Syst. Technol.*, vol. 4, pp. 627–640, Nov. 1996.

[10] F. L. Lewis, *Optimal Estimation*. New York: Wiley, 1986.

[11] M. Minsky, M. Ouh-young, O. Steele, F. P. Brooks Jr., and M. Behensky, "Feeling and seeing: Issues in force display," *Comput. Graphics*, vol. 24, no. 2, pp. 235–243, 1990.

[12] M. Ouhyoung, W. N. Tsai, M. C. Tsai, J. R. Wu, C. H. Wu, C. H. Huang, and T. J. Yang, "A low cost force feedback joystick and its use in PC video games," *IEEE Trans. Consumer Electron.*, vol. 41, pp. 787–793, Aug. 1995.

[13] J. Payette, V. Hayward, C. Ramstein, and D. Bergeron, "Evaluation of a force feedback haptic computer pointing device in zero gravity," in *Proc. 5th Annu. Symp. Haptic Interfaces Virtual Environments Teleoperator Syst.: Winter Annu. Meet. ASME*, Atlanta, GA, Nov. 1996, pp. 547–553.

[14] M. Rao, Q. Xia, and Y. Ying, *Modeling and Advanced Control for Process Industries*. New York: Springer-Verlag, 1993.

[15] L. Rabiner, M. Sambur, and C. Schmidt, "Applications of a nonlinear smoothing algorithm to speech processing," *IEEE Trans. Acoust., Speech, Signal Processing*, vol. ASSP-23, pp. 552–557, Dec. 1975.

[16] M. E. Van Valkenburg, *Introduction to Modern Network Synthesis*. New York: Wiley, 1960.